

Minerva Becker, MD
Francis Marchal, MD
Christoph D. Becker, MD
Pavel Dulguerov, MD
Georges Georgakopoulos,
MD
Willy Lehmann, MD
François Terrier, MD

Index terms:

Salivary glands, diseases, 264.818,
264.819
Salivary glands, MR, 264.121411,
264.121419
Salivary glands, radiography,
264.121411, 264.121419,
264.1222, 264.1298
Salivary glands, US, 264.1298

Radiology 2000; 217:347–358

Abbreviations:

EXPRESS = extended-phase
conjugate-symmetry rapid spin
echo
MIP = maximum intensity projection
3D = three dimensional

¹ From the Department of Radiology, Division of Diagnostic and Interventional Radiology (M.B., C.D.B., G.G., F.T.), and the Department of Otorhinolaryngology, Head and Neck Surgery (F.M., P.D., W.L.), Geneva University Hospital, rue Micheli-du-Crest 24, 1211 Geneva, Switzerland. Received September 8, 1999; revision requested October 8; final revision received January 19, 2000; accepted February 1. **Address correspondence to** M.B. (e-mail: cmbecker@vtx.ch).

© RSNA, 2000

Author contributions:

Guarantors of integrity of entire study, M.B., W.L., F.T.; study concepts and design, M.B., F.M., P.D.; definition of intellectual content, M.B., F.M., C.D.B.; literature research, M.B.; clinical studies, M.B., F.M., G.G.; data acquisition, M.B., F.M., G.G.; data analysis, M.B., C.D.B.; manuscript preparation, M.B.; manuscript editing, M.B., C.D.B.; manuscript review, P.D., F.T.

Sialolithiasis and Salivary Ductal Stenosis: Diagnostic Accuracy of MR Sialography with a Three-dimensional Extended-Phase Conjugate-Symmetry Rapid Spin-Echo Sequence¹

PURPOSE: To evaluate the accuracy of magnetic resonance (MR) sialography in detecting salivary glandular calculi and ductal stenoses.

MATERIALS AND METHODS: In a prospective study, 64 salivary glands in 61 consecutive patients with acute or recurrent parotid or submandibular glandular swelling were examined by using three-dimensional (3D) extended-phase conjugate-symmetry rapid spin-echo (EXPRESS) MR imaging. Transverse and sagittal-oblique source images and maximum intensity projection images were obtained. All MR images were analyzed independently by two radiologists, without knowledge of the final diagnosis. The reference standard was conventional sialography, ultrasonography (US), and sialendoscopy with or without surgery in 31 glands and was conventional sialography and US in 33 glands.

RESULTS: Final diagnoses included sialolithiasis ($n = 23$), sialolithiasis and stenosis ($n = 9$), stenosis without lithiasis ($n = 11$), early Sjögren syndrome without ductal stenosis ($n = 2$), ductal displacement ($n = 3$), and normal salivary glands ($n = 16$). The sensitivity, specificity, and positive and negative predictive values of MR sialography to detect calculi were 91%, 94%–97%, 93%–97%, and 91%, respectively. False-negative readings occurred due to calculi with a diameter of 2–3 mm in nondilated salivary ducts. Ductal stenosis was assessed, with a sensitivity of 100%, specificity of 93%–98%, positive predictive value of 87%–95%, and negative predictive value of 100%. Interobserver agreement was very good ($\kappa = 0.85$ – 0.97).

CONCLUSION: MR sialography with 3D EXPRESS imaging enables reliable prediction of salivary gland calculi and stenoses.

Although magnetic resonance (MR) imaging in the salivary glands is well established for the assessment of parenchymal lesions (1–7), to our knowledge reported data concerning its use in evaluating the ductal system still are limited (8–11). Because of its excellent delineation of the ductal system, conventional sialography currently is still considered the standard modality for assessing ductal abnormalities (12–15). However, ionizing radiation, dependence on the operator's technical skills for successful ductal cannulation, and the need for retrograde injection of contrast material are relative drawbacks of conventional sialography. Potential complications include rupture of the ductal system, activation of a clinically quiescent infection, and adverse reactions to contrast material (16). Catheter manipulation or the pressure of injection of contrast material may also result in the displacement of an anteriorly placed ductal stone into a position in which its retrieval by means of endoscopy or intraoral surgery becomes more difficult or even impossible (17).

Therefore, it appears desirable to use a less invasive yet reliable diagnostic examination for the salivary ducts in analogy to the biliary and pancreatic ducts in which the diagnostic accuracy of MR cholangiopancreatography in detecting calculi, stenoses, and anatomic variants has already been established (18–23).

Similar to MR cholangiopancreatography, MR sialography is based on the principle that stationary fluids are hyperintense on heavily T2-weighted images. After a preliminary report by Lomas et al (9), subsequent investigators have evaluated sequences to improve conspicuity of the ducts (10) and have demonstrated the MR sialographic findings of ductal displacement by mass lesions (11) and intraglandular collections of saliva in the context of Sjögren syndrome (24,25). At our institution, we have used a three-dimensional (3D) extended-phase conjugate-symmetry rapid spin-echo (EXPRESS) sequence since 1997. The purpose of the current study was to prospectively evaluate the diagnostic accuracy of MR sialography for the detection of sialolithiasis and salivary ductal stenosis.

MATERIALS AND METHODS

Patients

Between December 1997 and November 1999, 67 consecutive patients, with acute or recurrent salivary glandular swelling and no palpable mass, were enrolled in a prospective study, which included pretherapeutic MR sialography, conventional sialography, and ultrasonography (US). In addition, either for therapeutic purposes or for whenever conventional sialography was of inadequate quality, sialendoscopy with or without surgery was performed. Six patients were excluded from the study. In three patients, MR imaging could not be performed because of severe claustrophobia; in three other patients, conventional sialography was technically not feasible. The remaining 61 patients formed the basis of our study. The study protocol was approved by the institutional review board, and informed consent was obtained from all patients.

There were 42 men and 19 women, with a mean age of 44 years (age range, 6–85 years). Twenty-two patients had unilateral parotid glandular swelling, 36 patients had unilateral submandibular swelling, one patient had bilateral parotid glandular swelling, one patient had bilateral submandibular swelling, and one patient had submandibular and pa-

rotid swelling. Consequently, a total of 64 salivary glands were examined.

The standards of reference for assessing sialolithiasis, salivary ductal stenosis, or other salivary glandular abnormalities were conventional sialography, US and sialendoscopy with or without endoscopic stone removal or ductal dilatation in 27 (42%) of 64 salivary glands; conventional sialography, US, sialendoscopy, and surgery in four (6%) salivary glands; and conventional sialography and US in 33 (52%) salivary glands. To avoid confirmation bias, MR sialographic findings were not used in the decision to perform sialendoscopy or surgery. The final diagnoses were based on the conventional sialographic and US findings, as mentioned in the original radiology reports. In addition, endoscopy, laboratory, surgery, or pathology records, including results of labial gland biopsy, also were considered in the definitive diagnosis (made by F.M.).

MR Sialography

Depending on the availability of the MR imager, 32 patients underwent MR sialography prior to conventional sialography and US, while 29 patients underwent MR sialography after conventional sialography and US. MR sialography was performed by using a 1.5-T system (Eclipse; Marconi Medical Systems, Cleveland, Ohio), by using the standard quadrature transmit-receive head coil. The patients did not undergo any specific preparation and were asked to breathe quietly and refrain from coughing or vigorous swallowing during image acquisition. Rapid sagittal, coronal, and transverse localizers were obtained to facilitate section positioning. MR sialographic images were obtained in a transverse plane parallel to the hard palate and in a sagittal-oblique plane parallel to either the Wharton or Stensen duct. MR sialography was performed by using a 3D extended-phase conjugate-symmetry rapid spin-echo (3D-EXPRESS; Marconi Medical Systems) sequence, a heavily T2-weighted single-shot fast spin-echo sequence with half-Fourier analysis. Imaging parameters were optimized prior to the study by using healthy volunteers. The imaging parameters used in this series were a repetition time of 6,000–10,000 msec and an echo time of 190 msec (6,000–10,000/190), an echo-train length of 136, an interecho spacing of 8.5 msec, 2 × RAM, a field of view of 16 × 16 cm, a matrix of 256 × 256 pixels, a section thickness of 0.6–1.5 mm, and 5 minutes to 6 minutes 30 seconds per sequence. In

all patients, postprocessing of the MR sialographic images was performed at a separate workstation (Vistar; Marconi Medical Systems). Maximum intensity projection (MIP) reconstructions were obtained in all patients. All images were recorded as hard copies and archived on optical disks to enable image review directly on the computer screen by using variable window settings, if necessary.

Conventional Sialography

Conventional sialography was performed by using standard fluoroscopic equipment (Digital Spot Imaging Diagnost 96; Philips Medical Systems, Amsterdam, the Netherlands). Prior to study commencement, conventional radiographs were obtained in anteroposterior and lateral-oblique projections to detect grossly radiopaque sialoliths. To best visualize the intraoral opening of either the Stensen or Wharton duct, all patients received a secretagogue (fresh lemon) prior to study commencement. The sialographic equipment included a set of 00–0-caliber lacrimal dilators (Laubscher Medical Equipment, Höllstein, Switzerland), 0.012–0.021-inch sialographic cannulas (Manashil-type cannulas or modifications of butterfly needles; Cook Europe, Bjaeverskov, Denmark), a polyethylene connecting tube, a 5-mL syringe, and a low-osmolarity water-soluble contrast agent such as ioxaglate sodium and ioxaglate meglumine (Hexabrix 200; Guerbet, France) (12–14). Once the ductal opening was identified, the dilators were used to widen it for easier cannula placement. Then the cannula was advanced gently to avoid perforation, and 0.3–1.5 mL of contrast material was injected slowly by using manual pressure. The injection was always performed under fluoroscopic control to achieve optimum ductal filling, and spot radiographs were obtained in anteroposterior and lateral-oblique projections to document the examination. A radiograph was obtained at evacuation in all patients to document ductal emptying after repeat administration of fresh lemon.

US Technique

Gray-scale US in the salivary glands was performed in all patients by using a linear-array 7-MHz transducer (Acuson, Mountain View, Calif). US was performed at the same time as conventional sialography, and the findings from both examinations were reported together.

Image Interpretation

All MR images were reviewed separately by two experienced radiologists (M.B.,

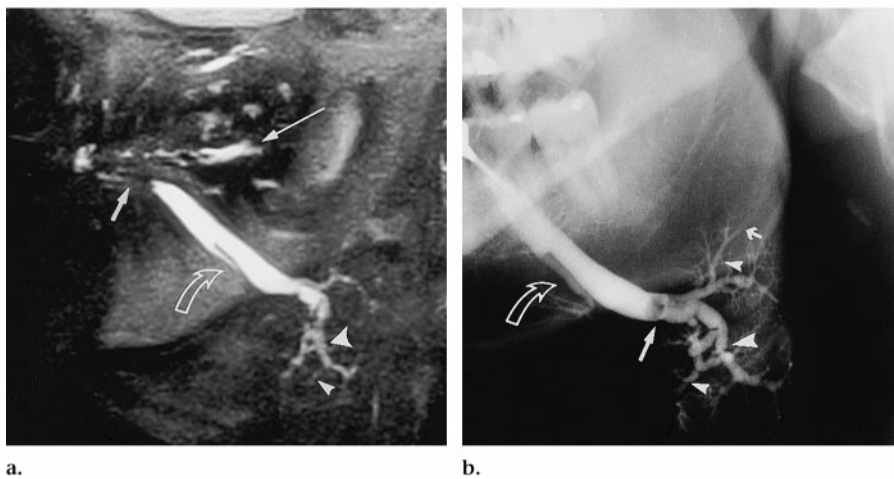


Figure 1. Images in a 26-year-old man at presentation with recurrent submandibular glandular swelling during mastication. (a) Sagittal-oblique 3D-EXPRESS MIP reconstruction (10,000/190; echo-train length, 136) shows a 4-mm stone near the orifice of the Wharton duct (thick arrow). Bartholin duct (curved arrow), primary branches (large arrowhead), and secondary intraglandular branches (small arrowhead) are slightly dilated. Hyperintense saliva is seen within the oral cavity (thin arrow). (b) Lateral-oblique conventional sialographic image obtained after MR sialography confirms the diagnosis of sialolithiasis and shows the distal displacement of the calculus (long straight arrow) caused by active filling of the ductal system. Bartholin duct (curved arrow) and primary (large arrowhead), secondary (small arrowheads), and tertiary branches (short straight arrow) are slightly dilated. The calculus was removed endoscopically.

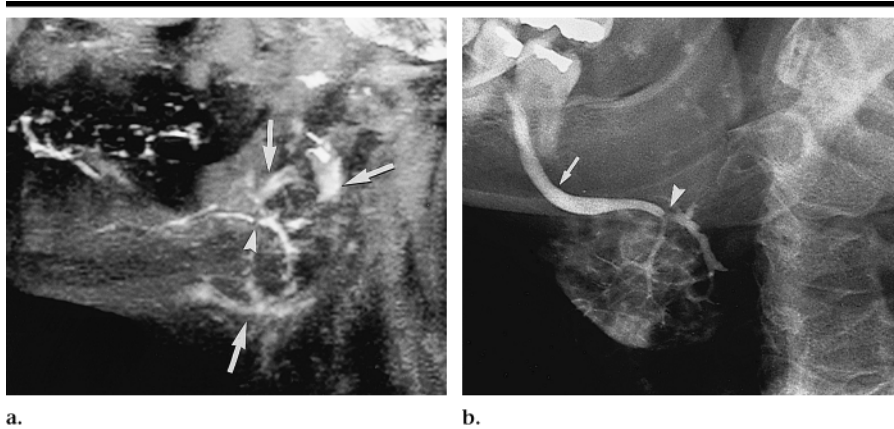


Figure 2. Images in a 45-year-old woman at presentation with recurrent submandibular glandular swelling during mastication. (a) Sagittal-oblique 3D-EXPRESS MIP reconstruction (10,000/190; echo-train length, 136) depicts a 2-mm calculus (arrowhead) within the Wharton duct at the level of the posterior edge of the mylohyoid muscle, with no associated ductal dilatation. Glandular parenchyma displays areas of increased signal intensity (arrows) on source images and MIP reconstructions. These areas had a low signal intensity on T1-weighted images and corresponded with associated sialadenitis. (b) Lateral-oblique conventional sialographic image confirms the presence of a 2-mm calculus (arrowhead). The proximal portion of the Wharton duct is better visualized because of retrograde filling of the ductal system (arrow). Sialendoscopy performed after conventional sialography confirmed the presence of a distal 2-mm calculus.

C.D.B.), in accordance with uniform criteria. Both reviewers were unaware of the clinical, conventional sialographic, US, endoscopic, and/or surgical results at the time of image interpretation. One of the reviewers (M.B.) is a head and neck radiologist, and the second reviewer (C.D.B.) is an abdominal radiologist with expertise in MR cholangiopancreatography. Both reviewers

regularly interpreted conventional sialographic images and therefore were familiar with the appearance of the conditions being studied. One radiologist (M.B.) reviewed the images prospectively, which resulted in the original clinical reports; he performed his assessment mainly at the workstation and thus was able to use post-processing, if necessary. The other radiolo-

TABLE 1
Results of MR Sialography for the Detection of Salivary Gland Calculi

Statistic	Reviewer 1	Reviewer 2
True-positive	29	29
True-negative	31	30
False-positive	1	2
False-negative	3	3
Sensitivity	29/32 (91)	29/32 (91)
Specificity	31/32 (97)	30/32 (94)
Positive predictive value	29/30 (97)	29/31 (94)
Negative predictive value	31/34 (91)	30/33 (91)
Accuracy	60/64 (94)	59/64 (92)

Note.—Data are the number of glands. Data in parentheses are percentages. Interobserver agreement was very good ($\kappa = 0.97$).

gist (C.D.B.) reviewed the images retrospectively on the basis of the hard copies. However, review of images directly on the computer screen, with variable window settings, was available if requested.

The criteria for detailed image interpretation were listed on each reviewer's evaluation sheet. Calculi were diagnosed when round, ovoid, or irregularly shaped signal voids were identified within or immediately next to a dilated or nondilated salivary duct. In addition, the reviewers indicated the precise position and diameter of calculi and whether one or multiple calculi were present within the ductal system. All MR images were interpreted together; however, whenever there was a discrepancy between source images and MIP images in interpretation regarding calculi, the interpretation of source images took precedence. Stenoses were diagnosed when an abrupt transition from ductal dilatation to signal void, a "string of sausages" (13–15), "tree in autumn" (13–15), or tapered appearance of the salivary ducts was seen. In the absence of ductal dilatation, failure to demonstrate the main submandibular or parotid ducts throughout their full length was not considered indicative of stenosis. As with calculi, all MR sialographic images were evaluated together; however, if there was a discrepancy between the source images and the MIP images in interpretation regarding stenoses, the interpretation of the MIP images took precedence. These evaluation criteria were defined beforehand and were based on our previous experience with interpretation of MR cholangiopancreatographic images (19). Both reviewers also assessed high-signal-intensity areas within the glandular parenchyma on T2-weighted images that

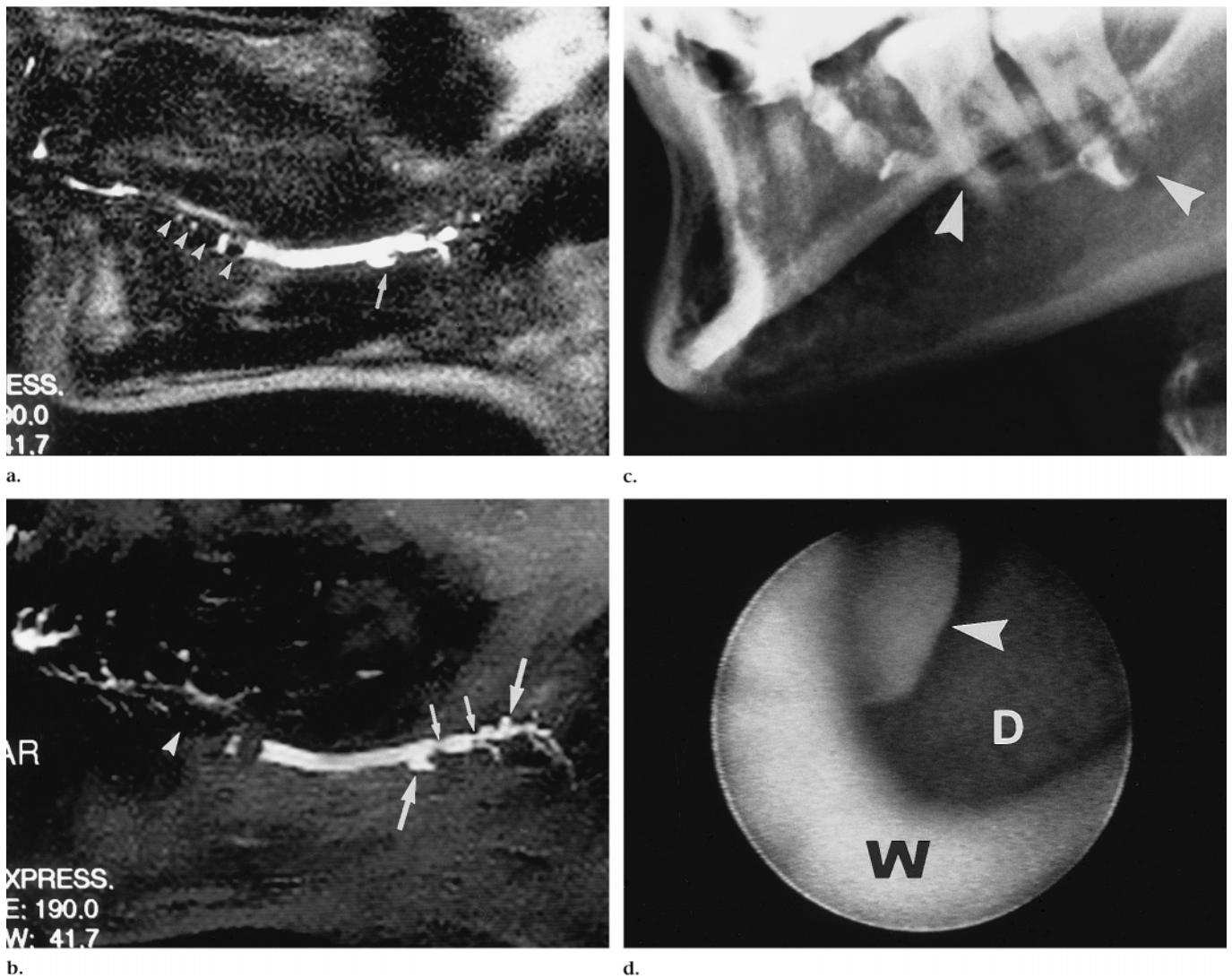


Figure 3. Images in a 39-year-old woman at presentation with recurrent submandibular glandular swelling during mastication. (a) Sagittal-oblique 3D-EXPRESS source image (8,000/190; echo-train length, 136) shows 2–4-mm stones (arrowheads) within the anterior third of the Wharton duct and shows ductal dilatation and associated sialodochitis with a small diverticular outpouching (arrow). (b) MIP reconstruction of a (8,000/190; echo-train length, 136) does not depict the calculi (arrowhead) near the orifice of the Wharton duct as clearly. However, the diverticular outpouchings (large arrows) and the irregular ductal caliber with areas of focal narrowing (small arrows) caused by inflammatory changes (sialodochitis) are better depicted than in a. (c) Lateral-oblique conventional sialographic image shows incomplete filling of the ductal system (arrowheads) that is caused by distal displacement of calculi. The remainder of the ductal system could not be visualized despite an increased injection pressure. (d) Sialendoscopic image obtained after conventional sialography confirms the presence of calculi, stenotic areas, and diverticular outpouchings. *D* = proximal diverticulum, *W* = Wharton duct. A 3-mm stone (arrowhead) was displaced into the proximal diverticulum during conventional sialography.

were suggestive of Sjögren syndrome (24,25). In addition, each reviewer noted anatomic variants, such as an accessory duct, and ductal displacement, diverticular outpouchings, ranulas, or tumors. An image was considered normal if the following criteria were fulfilled: absence of calculi; absence of ductal dilatation, with or without visualization of the entire ductal system; absence of high-signal-intensity areas within the glandular parenchyma that were suggestive of Sjögren syndrome; absence of ductal displace-

ment; and absence of ranulas, diverticular outpouchings, or tumors.

Statistical Analysis

The MR sialographic findings of each reviewer were compared with the final diagnoses. The sensitivity, specificity, positive and negative predictive values, and overall accuracy of MR sialography for the detection of sialolithiasis, salivary ductal stenosis, and disease in general were calculated for each reviewer. Inter-

observer variability was assessed by means of the κ statistic by using the STATA release 5 program for Unix (Stata, College Station, Tex). Interobserver agreement was interpreted as very good ($\kappa > 0.80$), good ($\kappa = 0.80-0.61$), moderate ($\kappa = 0.60-0.41$), fair ($\kappa = 0.40-0.21$), or poor ($\kappa \leq 0.20$).

RESULTS

The final diagnoses in all 64 salivary glands were sialolithiasis ($n = 23$); sialo-

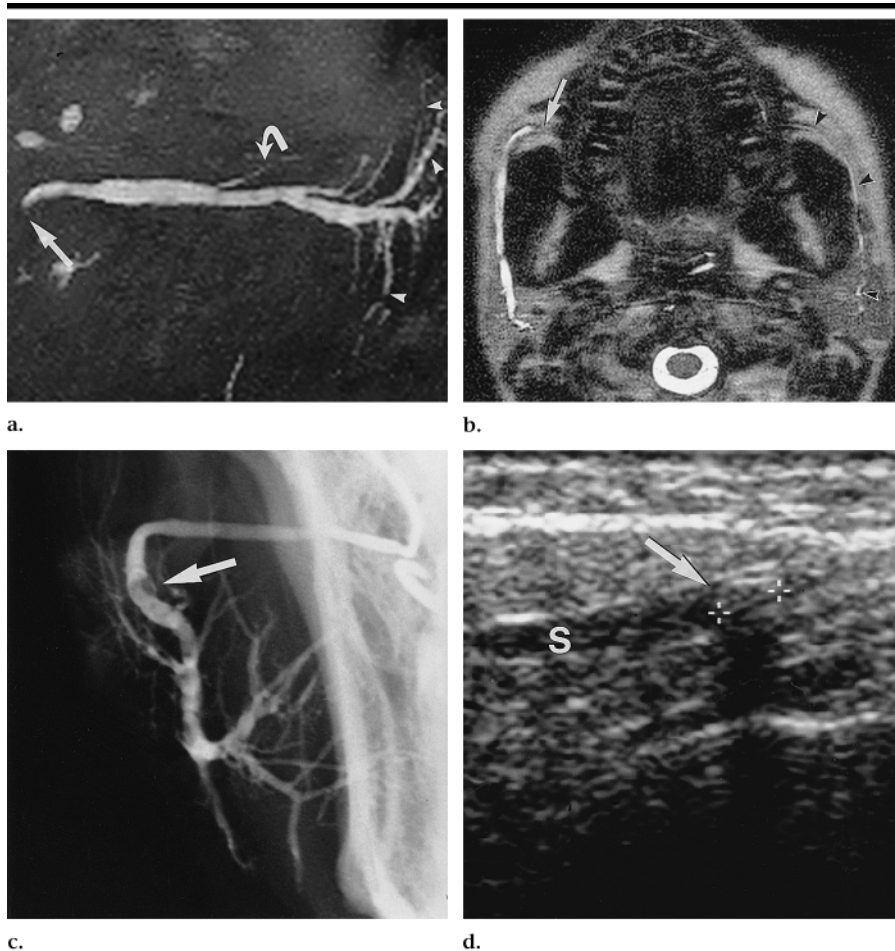


Figure 4. Image in a 27-year-old man at presentation with recurrent parotid swelling during mastication. (a) Sagittal-oblique 3D-EXPRESS MIP reconstruction (8,000/190; echo-train length, 136) shows dilatation of the Stensen duct in its entire course from the orifice (straight arrow) to its intraglandular branches (arrowheads). A short stenosis at the ductal orifice (straight arrow) was suspected by both reviewers. Curved arrow points to an accessory duct. (b) Transverse 3D-EXPRESS source image (8,000/190; echo-train length, 136) shows marked dilatation of the Stensen duct on the right. However, no filling defect is seen in its anterior portion near the orifice (arrow). Therefore, the diagnosis of stenosis was made again by both reviewers. Note, for comparison, the normal appearance of the Stensen duct on the left (arrowheads). (c) Anteroposterior conventional sialographic image obtained after MR sialography shows a filling defect that suggests a small calculus (arrow). (d) Transverse US image obtained after conventional sialography confirms the diagnosis of a 3-mm calculus (arrow), which was removed endoscopically. Crosshairs indicate borders of stone. S = dilated Stensen duct.

lithiasis, sialodochitis, and stenosis ($n = 9$); sialadenitis, sialodochitis, and stenosis without lithiasis, including glands in one patient with advanced Sjögren syndrome ($n = 11$); sialadenitis without sialodochitis in patients with early Sjögren syndrome ($n = 2$); ductal displacement caused by a plunging ranula ($n = 1$) or a Warthin tumor ($n = 2$); and normal salivary glands ($n = 16$).

Sialolithiasis

On the basis of the final diagnosis, sialolithiasis was present in 32 salivary glands (in the submandibular gland in 26

and in the parotid gland in six) and was absent in 32 glands. The largest diameter of the calculi was 3 mm or less in 12 (37.5%) glands; larger than 3 mm but smaller than or equal to 6 mm in 12 (37.5%) glands; larger than 6 mm but smaller than or equal to 9 mm in four (12.5%) glands; and larger than 9 mm in four (12.5%) glands. A single calculus was present in 20 salivary glands, whereas multiple calculi were present in 12 glands. Calculi were intraductal in 20 submandibular and four parotid glands and were intraparenchymal in six submandibular and two parotid glands. Par-

tial erosion of a calculus through the ductal wall in association with a chronic fibrotic reaction was seen in seven submandibular glands and in one parotid gland.

Results of MR sialography for the detection of sialolithiasis are summarized in Table 1. In 59 glands, both reviewers correctly assessed the presence of calculi. In 26 glands, calculi were associated with ductal dilatation, and in six glands, no ductal dilatation was seen at MR sialography (Figs 1–3). There were three false-positive MR sialographic assessments caused by short stenoses, which were interpreted as calculi in two instances by one reviewer and in one instance by the other reviewer. False-negative readings occurred in six instances (three false-negative assessments for each reviewer). Both reviewers missed 2- and 3-mm submandibular stones within the Wharton duct (at the level of the posterior edge of the mylohyoid muscle), which caused no ductal dilatation in two glands. Both calculi were removed endoscopically. In addition, both reviewers missed a 3-mm parotid stone, which was interpreted as a short stenotic area within the Stensen duct (Fig 4).

In the presence of ductal dilatation, the degree of dilatation as seen at MR sialography was inferior to that seen at conventional sialography in 25 glands. Discrepancies regarding the exact location of a calculus as assessed at MR sialography and conventional sialography were noted in seven cases. In these cases, active filling of the ductal system with contrast material during conventional sialography resulted in the displacement of an anteriorly placed ductal stone into a more posterior position (Fig 1). In seven glands, MR sialography was superior to conventional sialography because it enabled imaging of the upstream section of the ductal system, which was not visualized at conventional sialography (Fig 3). Interobserver agreement regarding the diagnosis of sialolithiasis was very good ($\kappa = 0.97$). Both reviewers found that the source images—particularly those acquired in the transverse plane—were crucial for the diagnosis of small calculi, because these calculi often were obscured on MIP reconstructions (Fig 5) by surrounding saliva.

Ductal Stenosis

On the basis of the final diagnosis, ductal stenosis was present in 20 salivary glands with sialodochitis (in the submandibular gland in eight; in the parotid

TABLE 2
Results of MR Sialography for the
Detection of Salivary Gland
Stenosis in 61 Glands

Statistic	Reviewer 1	Reviewer 2
True-positive	20	20
True-negative	43	41
False-positive	1	3
False-negative	0	0
Sensitivity	20/20 (1)	20/20 (1)
Specificity	43/44 (98)	41/44 (93)
Positive predictive value	20/21 (95)	20/23 (87)
Negative predictive value	43/43 (100)	41/41 (100)
Accuracy	63/64 (98)	61/64 (95)

Note.—Data are the number of glands. Data in parentheses are percentages. Interobserver agreement was very good ($\kappa = 0.85$)

gland in 12) and was absent in 44 salivary glands. In nine glands, stenoses were associated with sialolithiasis, and in 11 glands stenoses were seen in the absence of sialolithiasis. A single stenosis was present in seven salivary glands, whereas multiple stenoses were present in 13 glands. Stenoses were localized at the level of the main salivary ducts in 18 glands, at the level of the primary branching ducts in eight glands, and at the level of the secondary branching ducts in one gland.

The results of MR sialography in the detection of salivary ductal stenoses are summarized in Table 2. In 61 glands, both reviewers correctly assessed the presence or absence of stenosis, and in all glands, stenosis was associated with ductal dilatation at MR sialography (Figs 6, 7). There were four false-positive MR sialographic assessments regarding stenosis (one false-positive assessment by reviewer 1, and three false-positive assessments by reviewer 2). Both reviewers interpreted a 3-mm calculus as a short stenosis (Fig 4), and one of the reviewers interpreted two normal glands as having minor degrees of ductal stenosis. The degree of ductal dilatation seen at MR sialography and caused by stenosis was similar to the degree of dilatation seen at conventional sialography (Figs 6, 7). No discrepancies regarding the exact location of a stenotic area as assessed at MR sialography and conventional sialography were noted. However, conventional sialography enabled better visualization of the secondary and tertiary ducts in seven glands. In six glands with sialodochitis, diverticular outpouchings were observed at MR sialography. These were confirmed endoscopically and/or

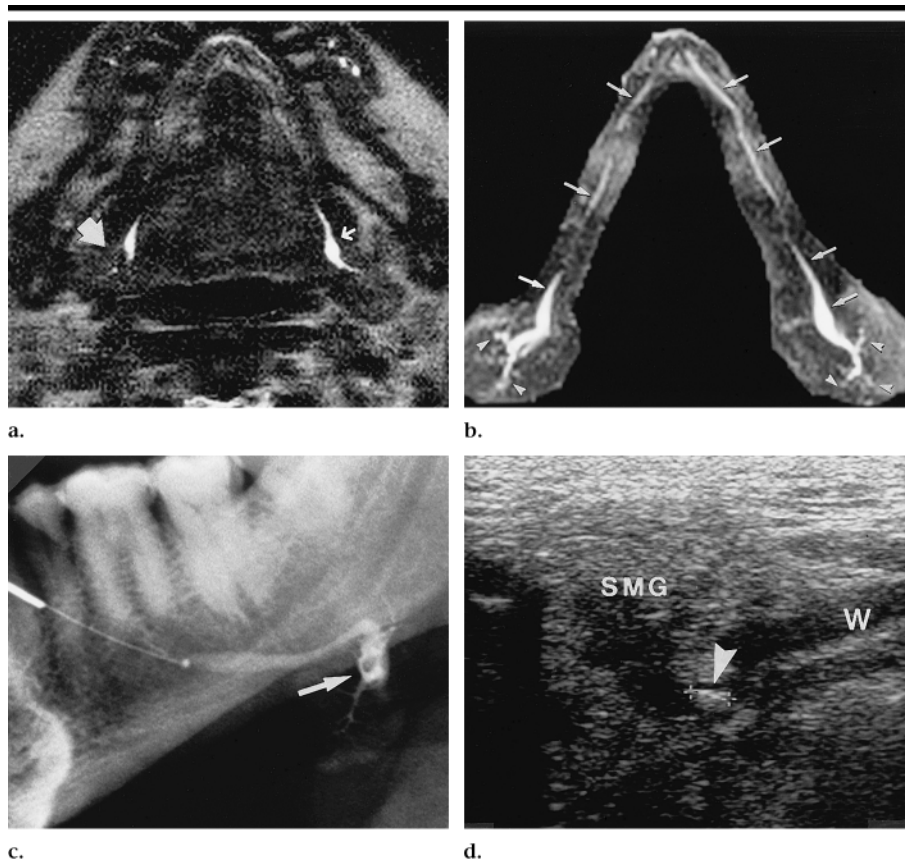


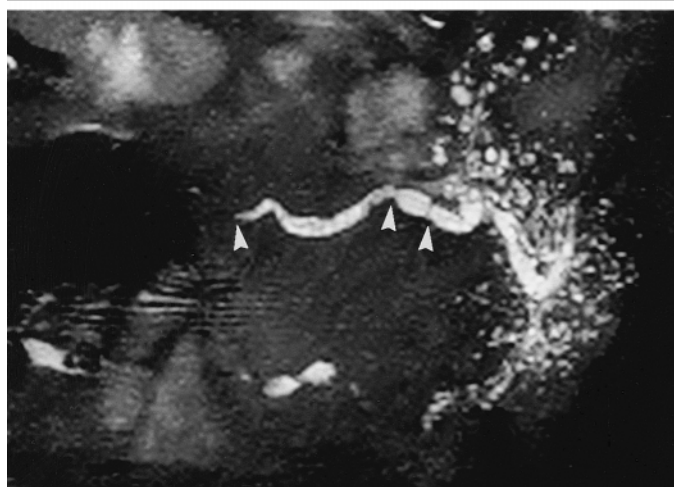
Figure 5. Images in a 37-year-old man at presentation with recurrent right-sided submandibular glandular swelling during mastication. (a) Transverse 3D-EXPRESS source image (8,000/190; echo-train length, 136) shows a 3-mm calculus (large arrow) in the right Wharton duct at the level of the posterior edge of the mylohyoid muscle. Small arrow points to the normal opposite Wharton duct. (b) MIP reconstruction of a (8,000/190; echo-train length, 136) shows a normal aspect of both the right and left Wharton duct (arrows) and no dilatation of the intraglandular branches (arrowheads). The calculus, clearly visualized in a, is obscured by surrounding saliva. (c) Lateral-oblique conventional sialographic image obtained after MR sialography shows a filling defect that corresponds to a small calculus (arrow). (d) Submental US image obtained after conventional sialography confirms the diagnosis of a 3-mm calculus (arrowhead), which was removed endoscopically. Crosshairs indicate lateral borders of the stone. SMG = submandibular gland, W = Wharton duct.

by means of conventional sialography (Fig 3). Interobserver agreement regarding the diagnosis of ductal stenosis was very good ($\kappa = 0.85$). Both reviewers found that the MIP reconstructions—particularly those images obtained in the sagittal-oblique plane—were essential for the diagnosis of stenoses because they yielded information that was displayed in projections that were similar to projections of images acquired with conventional sialography.

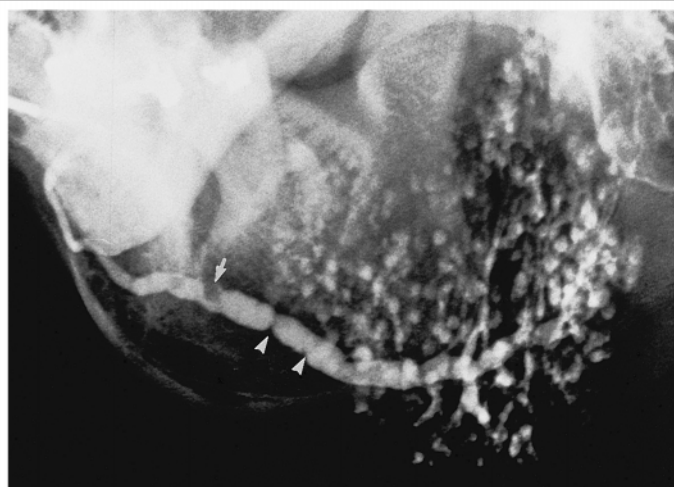
Normal versus Abnormal Salivary Glands

On the basis of the final diagnosis, 16 salivary glands were normal (four parotid glands and 12 submandibular glands). Abnormalities (regardless of their cause)

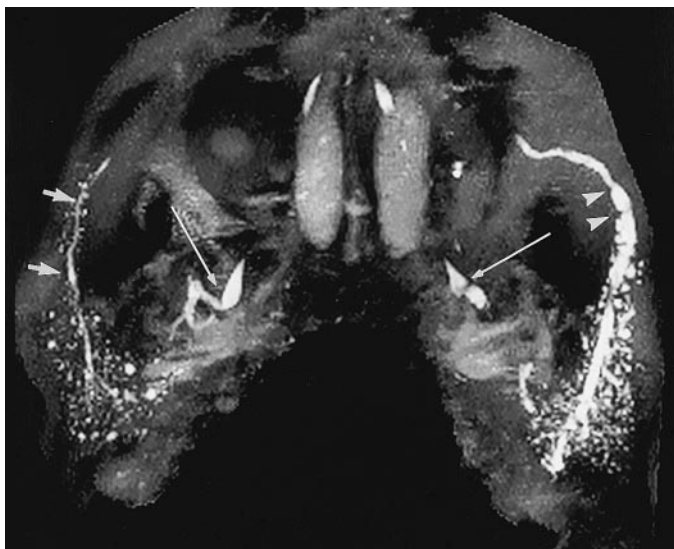
were present in 48 glands. The results of MR sialography for distinguishing normal from abnormal salivary glands are summarized in Table 3. In 61 glands, both reviewers correctly assessed the presence or absence of glandular abnormalities. Four false-negative readings occurred (two for each reviewer) and were caused by small calculi. The three cases with displacement of normal salivary ducts by plunging ranula and Warthin tumor (Fig 8) were correctly assessed by both reviewers. In two patients with autoimmune parotitis and normal main parotid ducts, the correct diagnosis was made by both reviewers on the basis of punctate (<1-mm) or cavitory (>2-mm) high-signal-intensity areas within the glandular parenchyma on T2-weighted



a.



c.



b.

Figure 6. Images in a 71-year-old man at presentation with recurrent left-sided parotid swelling. (a) Sagittal-oblique 3D-EXPRESS MIP reconstruction (8,000/190; echo-train length, 136) shows multiple 1–2-mm high-signal-intensity areas within the glandular parenchyma and a dilated and lobulated main duct with stenotic areas (arrowheads). (b) Transverse 3D-EXPRESS MIP reconstruction (10,000/190; echo-train length, 136) shows bilateral disease, with 1–2-mm intraglandular collections of saliva in the left parotid gland and multiple intraglandular saliva collections of 1 mm or smaller in the right parotid gland, a normal right Stensen duct (short arrows), marked dilatation and multiple stenoses (arrowheads) of the left main parotid duct, and dilatation and stenoses of both submandibular ducts (long arrows). (c) Lateral-oblique conventional sialographic image in the symptomatic left parotid gland confirms MR sialographic findings of contrast material extravasation within the glandular parenchyma and a dilated and lobulated main duct with stenotic areas (arrowheads). Arrow points to an air bubble, which has a characteristic appearance on fluoroscopic images—it deforms and moves rapidly during contrast material injection. Sialendoscopy in the left parotid gland confirmed the presence of multiple stenoses and the absence of calculi. The final diagnosis was Sjögren syndrome.

images. Conventional sialographic findings confirmed the diagnosis of stage 1 (punctate) Sjögren syndrome in the first patient and stage 3 (cavitary) Sjögren syndrome in the second patient.

In 15 cases, both reviewers correctly diagnosed normal glands. The main ducts were clearly visualized on MIP images in all normal salivary glands either at full length ($n = 11$) or at only partial length ($n = 4$). The Wharton duct was not visualized in four cases at the level of its anterior third within the floor of the mouth on MIP images. However, careful analysis of 0.6-mm EXPRESS source images revealed a duct with a caliber of less than 1 mm and regular contours. Primary branching ducts were visible within all normal submandibular glands and in three of four normal parotid glands (Fig 9). Secondary branching ducts were visible in three normal parotid glands and in

six normal submandibular glands, while tertiary branching ducts were seen in only one normal parotid gland. There was one false-positive assessment caused by slight asymmetry of the extraglandular portion of the Stensen duct, which was interpreted as a minor degree of dilatation. Anatomic variants (accessory ducts) were present in 19 of 64 glands (prevalence, 30%) and were identified at MR sialography in 15 glands (Figs 2, 9). Interobserver agreement regarding the diagnosis of salivary gland abnormality in general was very good ($\kappa = 0.96$).

DISCUSSION

Acute and recurrent submandibular or parotid swelling is a common symptom and may indicate a variety of salivary glandular abnormalities, such as viral or

bacterial infection; calculi; secondary infection due to ductal obstruction, with subsequent ductal strictures; and autoimmune disease. The traditional treatment for salivary stones has been surgical intraoral extraction, which usually is associated with meatotomy or dochoplasty, whereas recurrent postobstructive sialadenitis after failed intraoral stone extraction usually is treated with sialadenectomy (13,26–30). Several new techniques have recently become available to treat sialolithiasis and salivary duct stenosis by way of an intraluminal approach and include extracorporeal sialolithotripsy, endoscopic stone removal, lithotripsy, and endoluminal balloon dilatation. Although the increasing use of these techniques greatly reduces the risk of facial or lingual nerve damage that is involved with sialadenectomy, it also enhances the need for precise pretherapeutic mapping of the salivary duct system (12,13,26,27,29,31–34). Ideally, imaging should be noninva-

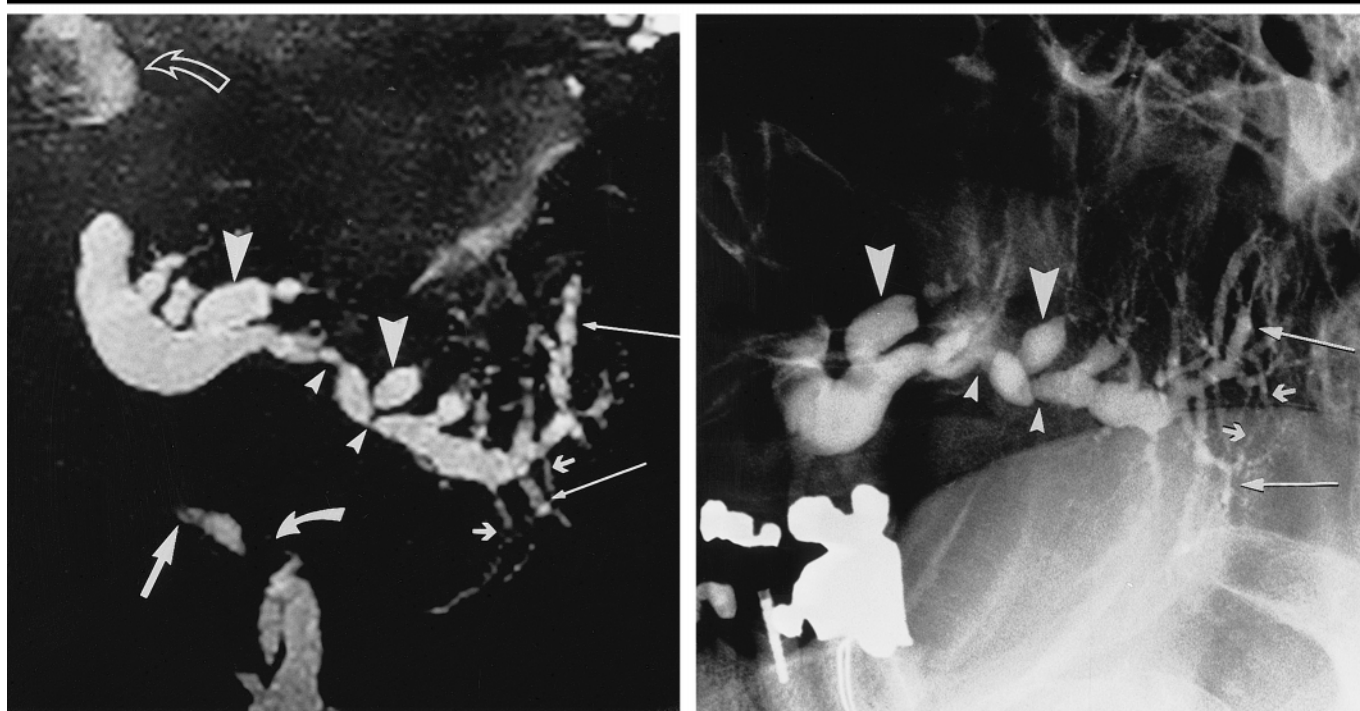


Figure 7. Images in a 65-year-old woman at presentation with recurrent left-sided parotid swelling. **(a)** Sagittal-oblique 3D-EXPRESS MIP reconstruction (10,000/190; echo-train length, 136) shows a dilated and lobulated main duct with stenotic areas (small arrowheads) and diverticular outpouchings (large arrowheads). Minor variations in the caliber of primary and secondary intraglandular branches (long thin arrows = large caliber, short arrows = narrow caliber) correspond to dilated and stenotic areas, respectively. As incidental findings, note also the marked dilatation, stenosis (long thick arrow), and calculus (solid curved arrow) in the left Wharton duct. A hyperintense area above the Stensen duct (open curved arrow) corresponds with retained mucus in the maxillary sinus. **(b)** Lateral-oblique conventional sialographic image in the left parotid gland confirms MR sialographic findings of marked dilatation of the main duct, with stenotic areas (small arrowheads) and diverticular outpouchings (large arrowheads). Minor variations in the caliber of primary and secondary intraglandular branches (long arrows = large caliber, short arrows = narrow caliber) that correspond to dilated and stenotic areas, respectively, and better visualization of secondary and tertiary branches due to active filling with contrast material also are noted.

sive, so that endoluminal instrumentation can be combined with the benefit of treatment.

Imaging techniques in the salivary glands include conventional radiography, US, computed tomography (CT), MR imaging, and conventional sialography. Conventional radiography has long been performed to detect salivary stones but has been almost completely replaced. High-resolution US is used as a noninvasive first-line examination to assess the presence of ductal dilatation and calculi (26,31). At many institutions, US is combined with conventional sialography, and the evaluation of the ductal system is based on the information obtained from both examinations, as is the case at our institution. Although multiple small parotid nodules in patients with autoimmune sialadenitis may be seen readily at CT, and although focused helical CT with 1–2 mm collimation may depict even tiny calculi, CT is of limited use in suspected abnormalities of the salivary ducts, since it requires retrograde injection

of contrast material, and image resolution is inferior as compared with that of conventional sialography (13,14,35).

Conventional sialography continues to provide high-spatial-resolution images in the salivary ducts. To our knowledge, it is currently considered to be the only imaging modality for examining the fine anatomy of the salivary ducts and for assessing the presence of ductal abnormalities. The most common indications for conventional sialography are small sialoliths or foreign bodies, strictures, fistulas, diverticula, changes secondary to trauma or infection, communicating cysts, autoimmune diseases, and sialosis (13–15,26). Advantages include multiplanar imaging, assessment of ductal function as a response to a sialogogue, and occasional therapeutic success of stone release after retrograde injection of contrast material. Disadvantages include irradiation, the need for an experienced operator to cannulate the small, often edematous ductal orifices, and pain during retrograde injection of contrast material.

TABLE 3
Results of MR Sialography for the Detection of General Salivary Gland Abnormality

Statistic	Reviewer 1	Reviewer 2
True-positive	46	46
True-negative	16	15
False-positive	0	1
False-negative	2	2
Sensitivity	46/48 (96)	46/48 (96)
Specificity	16/16 (100)	15/16 (94)
Positive predictive value	46/46 (100)	46/47 (98)
Negative predictive value	16/18 (89)	15/17 (88)
Accuracy	62/64 (97)	61/64 (95)

Note.—Data are the number of glands. Numbers in parentheses are percentages. Interobserver agreement was very good ($\kappa = 0.96$).

Acute salivary infection is an absolute contraindication, and potential complications of conventional sialography include damage to the orifice, overfilling and rupture of the ductal system, exacerbation

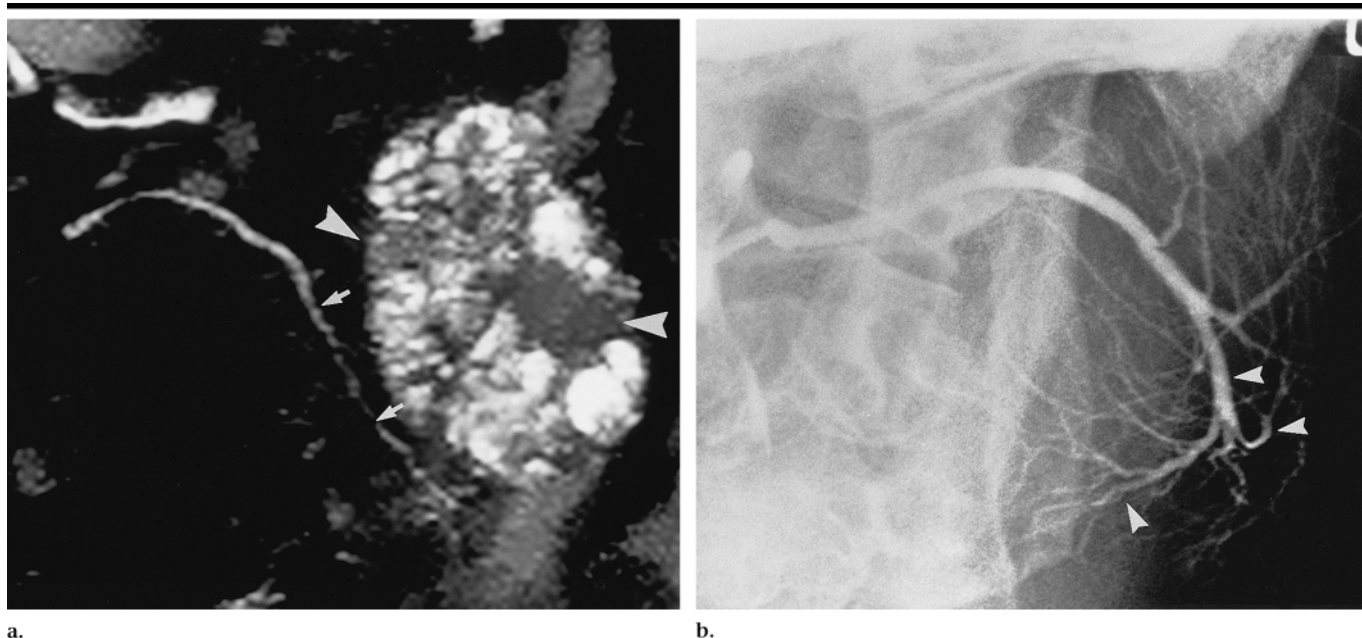


Figure 8. Images in a 73-year-old man at presentation with recurrent left-sided parotid swelling. (a) Sagittal-oblique 3D-EXPRESS MIP reconstruction (10,000/190; echo-train length, 136) shows displacement of a normal main parotid duct (arrows) by a large mass with hyperintense and hypointense (arrowheads) areas. The T1-weighted spin-echo image (not shown) depicted large cystic and hemorrhagic areas that suggested a Warthin tumor. (b) Lateral-oblique conventional sialographic image in the left parotid gland shows an abnormal course of the left main parotid duct and its intraglandular branches, which are displaced inferolaterally (arrowheads). The orientation in the sagittal plane of the MR sialogram and the conventional sialogram is slightly different and results in different projections. The parotid ducts have a normal caliber. Surgery confirmed the displacement of normal parotid ducts by a Warthin tumor.

tion of infection, and adverse reaction to contrast material (13,14,16). Failure to cannulate the ductal orifice may occur in the presence of a calculus at the ductal orifice, with related edema of the surrounding buccal mucosa or in the absence of any ductal abnormalities. Smaller calculi and subtle ductal abnormalities near the ductal orifice may be obscured by the injection of contrast material, and overfilling may result in a false-positive diagnosis of sialectasis. The injection of contrast material may also result in the displacement of an anterior ductal stone into a posterior position, in which it can no longer be reached by means of an intraoral surgical approach or in which endoscopic removal is more difficult (17,26,27). These disadvantages of conventional sialography may explain the search for a noninvasive diagnostic examination.

Although MR imaging is used widely to evaluate parenchymal lesions of the major salivary glands, dedicated sequences for adequate visualization of the salivary ducts have been developed only recently. MR sialography uses an exceptionally long echo time and a long echo train length to obtain heavily T2-weighted images within a reasonable acquisition period. Because of the

T2 decay during data acquisition, tissues with a short T2 produce practically no signals in the echoes at the end of the pulse train. Different sequences have been used for MR sialography. Lomas et al (9) reported their first clinical experience with MR sialography by using a modification of a standard rapid acquisition with relaxation enhancement, or RARE, sequence in healthy volunteers and three patients. Murakami et al (10) recently reported good visualization of the salivary ducts by using a single-shot turbo spin-echo sequence in 12 patients, and Ohbayashi et al (24) used a T2-weighted gradient and spin-echo, or GRASE, sequence. We have modified a standard 3D rapid spin-echo sequence for MR sialography. This sequence has the advantage of allowing the acquisition of thin sections for the detection of small stones and MIP images for the visualization of the overall ductal anatomy. Most of the signal related to vascular motion and most of the adjacent tissue signal are removed. We did not use additional spectral fat suppression to improve background suppression; we found that discrete background visualization of anatomic structures on MIP reconstructions was helpful because it facilitates orientation

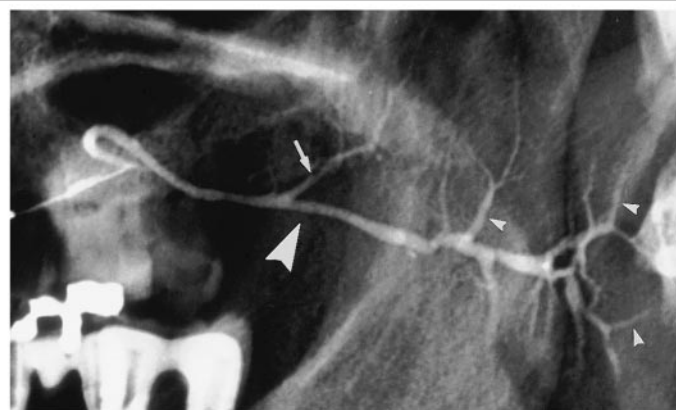
to surrounding structures. By using this sequence, diagnostic-quality images were obtained in all cases; the only failures were due to claustrophobia.

To the best of our knowledge, at the time this article was written, few data were available with which to assess the clinical usefulness of MR sialography for the different abnormal conditions. Investigators in a recent study (11) described the changes seen in a series of patients with predominantly neoplastic disease, and Ohbayashi et al (24) described the MR sialographic findings in patients suspected to have Sjögren syndrome.

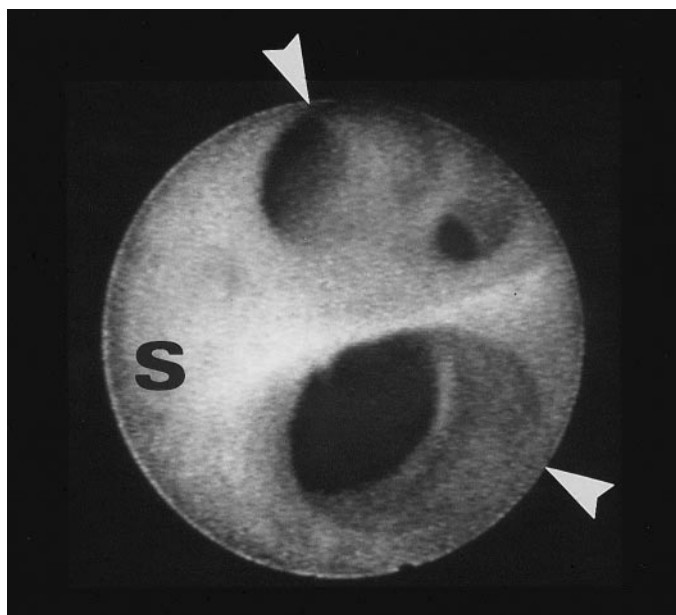
On the basis of the results of our series, several advantages of MR sialography become evident. Because we were dealing with a relatively young population with benign salivary glandular diseases, the lack of ionizing radiation appears to be an important advantage. In addition, MR sialography can be performed in patients in the acute stage and also in patients with known reactions to iodinated contrast material. In our own series, conventional sialography was technically not feasible in three (4%) of 67 glands because of our failure to cannulate the ductal orifice. In addition, in seven (11%) of 64 glands, MR sialography revealed additional information by allowing better vi-



a.



b.



c.

Figure 9. Images in a 54-year-old woman at presentation with acute left-sided parotid swelling. (a) Sagittal-oblique 3D-EXPRESS MIP reconstruction (10,000/190; echo-train length, 136) shows a normal main parotid duct (large arrowhead) with a 1-mm diameter and normal primary branches (small arrowheads) and shows a normal accessory duct (straight arrow) with a diameter of less than 1 mm. Hyperintense saliva (curved arrow) is seen within the oral cavity. (b) Lateral-oblique conventional sialographic image obtained after MR sialography confirms the diagnosis of normal ducts. The main parotid duct (large arrowhead), the accessory duct (arrow), and the primary and secondary branches (small arrowheads) appear slightly larger than on MR sialographic images because of active filling with contrast material. (c) Because the patient complained of persistent swelling and discomfort after conventional sialography, sialendoscopy was performed to rule out a small mucous plug and confirmed a normal-appearing main duct (S), primary branches (arrowheads), and secondary branches (not shown).

sualization of the upstream portion of the salivary ducts (Fig 3), and in three (5%) of 64 glands in which conventional sialography showed displacement of normal ducts, MR sialography enabled the definitive diagnosis, namely, a Warthin tumor (Fig 9) and plunging ranula. Therefore, in 13 (19%) of 67 glands, MR sialography was superior to conventional sialography.

In our series, the diameter of calculi was less than or equal to 3 mm in 12 (37.5%) of 32 glands with calculi. All of these calculi were symptomatic, and the patients were scheduled for endoscopic stone removal, since the current therapeutic attitude of otorhinolaryngologists at our institution includes the removal of all symptomatic ductal calculi, regardless of their size. Although most of these small calculi were reliably diagnosed by

using MR sialography (Figs 2, 5), false-negative readings may occur in patients with 2–3-mm stones that are causing no ductal dilatation. We also have to consider that, in theory, MR sialography does not enable the distinction of solid calculi from inspissated mucus and/or debris, since the latter may also cause intraductal areas of signal void. From a practical point of view, however, this distinction would be of minor effect, since, in a patient with symptoms, endoscopic removal usually would be indicated in both situations. Small calculi were displayed best on transverse source images. On MIP images, small calculi may be obscured because of volume averaging, with surrounding hyperintense saliva (Fig 5). Therefore, careful analysis of both source and MIP images is mandatory.

To evaluate the diagnostic perfor-

mance of MR sialography, we used a very strict reference standard that implied the performance of several investigations, which included sialendoscopy. In fact, sialendoscopy proved to be superior to conventional sialography in three cases in which it not only was used to confirm the presence of calculi but also to show additional calculi in small side branches; these were retrieved endoscopically at the same time.

The results obtained with our examination technique appear promising. The sensitivity of MR sialography for detecting sialolithiasis was 91% for both reviewers, and the specificity was 94%–97%. Although sialolithiasis may be detected with US or 1-mm helical CT (35), nine (28%) of 32 glands with lithiasis in our series had associated single or multiple stenoses that necessitated additional endoscopic dilatation. These concomitant stenoses would have been missed if US or CT alone had been used. In these cases, a precise pretherapeutic diagnosis could be made only with either conventional sialography or MR sialography, thus facilitating pretherapeutic planning.

Stenosis in a major salivary glandular duct may occur secondary to a calculus,

with or without associated recurrent infection, in patients with chronic recurrent sialadenitis or later stages of autoimmune disease (6,13,14). Less often, trauma or ill-fitting dentures may cause stenosis. The sensitivity of MR sialography for detecting stenosis in our series was 100% for both reviewers, and the specificity was 93%–98%. The level of stenosis was defined precisely in all cases and corresponded to the level of stenosis identified at conventional sialography and sialendoscopy. Although in our series conventional sialography allowed better visualization of the peripheral ducts as compared with MR sialography, the sensitivity of MR sialography for detecting stenoses was not impaired. Stenoses were best diagnosed on MIP images, and, in most cases, the diagnosis was straightforward. The results of our series indicate that nonvisualization of the Wharton duct in its anterior third at the level of the floor of the mouth and of the Stensen duct in its portion overlying the masseter muscle on MIP reconstructions is a physiologic finding and should not be considered to be indicative of stenosis in the absence of ductal dilatation.

The diagnosis of Sjögren syndrome was straightforward in our series and was based on the identification of a punctate or cavitory appearance of the parotid glands. In a recent study (24) based on 35 patients suspected of having Sjögren syndrome, MR sialography had both a sensitivity and specificity of 100% in the diagnosis of Sjögren syndrome. However, the stage of salivary gland disease determined with MR sialography correlated with that determined with conventional sialography only in 89% of patients (24). In the remaining 11%, the authors noted discrepancies between conventional sialographic and MR sialographic images. Better visualization of peripheral ducts and a higher degree of dilatation at conventional sialography compared with MR sialography—as observed in our series—may be explained by the fact that conventional sialographic images are obtained after retrograde filling with contrast material, whereas MR sialographic images are obtained by depicting the saliva within the ducts. The latter may reflect a more realistic ductal diameter than artifactual dilatation of the ductal system, which may occur with conventional sialography.

Disadvantages of MR sialography include general MR imaging contraindications; distortion artifacts caused by dental amalgam may impair visualization of calculi or stenoses near the main ductal

orifice. However, dental amalgam did not impair diagnosis in our series. Despite the inferior resolution of MR sialography as compared with conventional sialography, especially for the assessment of secondary and tertiary ducts, diagnosis was not affected in our series.

In summary, the results of our study indicate that MR sialography with a 3D-EXPRESS sequence allows consistent and accurate assessment of salivary glandular calculi and stenoses. With the protocol used in our series, images of consistent quality may be obtained. MR sialography appears to be sufficiently accurate for recommendation as a noninvasive method in patients suspected to have salivary ductal disorders. In fact, we have begun to substitute MR sialography for conventional sialography in patients with acute or recurrent salivary glandular swelling. However, normal MR sialographic findings do not allow the exclusion of 2–3-mm calculi that cause no ductal dilatation. Therefore, in the small subset of patients with persistent symptoms and normal MR sialographic findings, we proceed to perform conventional sialography and US.

Acknowledgments: We thank Frank Henri, RT, and Robert Anderson, PhD, for technical assistance with imaging sequences, and Shu Fang Hsu-Schmitz, PhD, for statistical analysis.

References

- Mandelblatt SM, Braun IF, Davis PC, Frey SM, Jacobs LH, Hoffman JC. Parotid masses: MR imaging. *Radiology* 1987; 163:411–414.
- Mees K, Vogl T, Kellerman O. MRI of salivary glands. *Laryngol Rhinol Otol* 1988; 67:355–361.
- Tabor EK, Curtin HD. MR of the salivary glands. *Radiol Clin North Am* 1989; 27:379–392.
- Casselmann JW, Mancuso AA. Major salivary gland masses: comparison of MR imaging and CT. *Radiology* 1987; 163:183–189.
- Freling NJM, Molenaar WM, Vermey A, et al. Malignant parotid tumors: clinical use of MR imaging and histologic correlation. *Radiology* 1992; 185:691–696.
- Weissmann JL. Imaging of the salivary glands. *Semin Ultrasound CT MR* 1995; 16:546–568.
- Vogl TJ, Dresel SH, Spath M, et al. Parotid gland: plain and gadolinium-enhanced MR imaging. *Radiology* 1990; 177:667–674.
- Thibault F, Halimi P, Bely N, et al. Internal structure of the parotid gland at MR imaging: facial nerve or ductal system. *Radiology* 1993; 188:701–704.
- Lomas DJ, Carroll NR, Johnson G, Antoun NM, Freer CEL. MR sialography: work in progress. *Radiology* 1996; 200:129–133.
- Murakami R, Baba Y, Nishimura R, et al. MR sialography using half Fourier acqui-

- sition single shot turbo spin echo (HASTE) sequences. *AJNR Am J Neuroradiol* 1998; 19:959–961.
- Jungehülsing M, Fischbach R, Schröder U, Kugel H, Brochhagen HG, Eckel HE. Imaging case study of the month: magnetic resonance sialography. *Ann Otol Rhinol Laryngol* 1998; 107:530–535.
- Buckenham TM, George CD, McVicar D, Moody AR, Coles GS. Digital sialography: imaging and intervention. *Br J Radiol* 1994; 67:524–529.
- Morse MH. Salivary gland imaging. In: deBurgh Norman JE, McGurk M, eds. *Color atlas and text of the salivary glands: diseases, disorders, and surgery*. St Louis, Mo: Mosby, 1995; 105–127.
- Som PM, Brandwein M. Salivary glands. In: Som PM, Curtin HD, eds. *Head and neck imaging*. Vol 2. 3rd ed. St Louis, Mo: Mosby-Year Book, 1996; 825–914.
- Som PM, Shugar JMA, Train JS, et al. Manifestations of parotid gland enlargement: radiographic, pathologic, and clinical correlations. I. The autoimmune pseudo-sialectasias. *Radiology* 1981; 141:415–419.
- Cockrell DJ, Rout P. Adverse reaction following sialography. *Dentomaxillofac Radiol* 1993; 22:41–42.
- Seward GR. Anatomic surgery for salivary calculi. II. Calculi in the anterior part of the submandibular duct. *Oral Surg Oral Med Oral Pathol Oral Radiol Endod* 1968; 28:287–293.
- Laubenberger J, Büchert M, Schneider B, Blum U, Hennig J, Langer M. Breath-hold projection magnetic resonance cholangiopancreatography (MRCP): a new method for the examination of bile and pancreatic ducts. *Magn Reson Med* 1995; 33:18–23.
- Becker CD, Grossholz M, Becker M, Mentha G, dePeyer R, Terrier F. Choledocholithiasis and bile duct stenosis: diagnostic accuracy of MR cholangiopancreatography. *Radiology* 1997; 205:523–530.
- Becker CD, Grossholz M, Mentha G, de Peyer R, Terrier F. Magnetic resonance cholangiopancreatography: technique, potential indications, and diagnostic features of benign, postoperative, and malignant conditions. *Eur Radiol* 1997; 7:865–874.
- Holzknicht N, Gauger J, Sackmann M, et al. Breath-hold MR cholangiography with snapshot techniques: prospective comparison with endoscopic retrograde cholangiography. *Radiology* 1998; 206:657–664.
- Reinhold C, Taourel P, Bret PM, et al. Choledocholithiasis: evaluation of MR cholangiography for diagnosis. *Radiology* 1998; 209:435–442.
- Fulcher AS, Turner MA, Capps GW, Zfass AM, Baker KM. Half-Fourier RARE MR cholangiopancreatography: experience in 300 subjects. *Radiology* 1998; 207:21–32.
- Ohbayashi N, Yamada I, Yoshino N, Sasaki T. Sjögren syndrome: comparison of assessments with MR sialography and conventional sialography. *Radiology* 1998; 209:683–688.
- Tonami H, Ogawa Y, Matoba M, et al. MR sialography in patients with Sjögren's syndrome. *AJNR Am J Neuroradiol* 1998; 19:1199–1204.
- Marchal F, Becker M, Kurt AM, Lehmann W. Lithiases salivaires: nouvelles orienta-

- tions diagnostiques et thérapeutiques. *Méd et Hyg* 1997; 55:2064–2069.
27. Marchal F, Becker M, Vavrina J, Dulgerov P, Lehmann W. Diagnostic et traitement des sialolithiases. *Bull Méd Suisses* 1998; 79:1023–1028.
 28. Rontal M, Rontal E. The use of sialodochoplasty in the treatment of benign inflammatory obstructive submandibular gland disease. *Laryngoscope* 1987; 97:1417–1421.
 29. Dulgerov P, Marchal F, Lehmann W. Postparotidectomy facial nerve paralysis: possible etiologic factors and results with routine facial nerve monitoring. *Laryngoscope* 1999; 109:754–762.
 30. Goudal JY, Bertrand JC. Complications des traitements chirurgicaux de la lithiase sous-maxillaire. *Rev Stomatol Chir Maxillofac* 80:3439–3450.
 31. Ottaviani F, Capaccio P, Rivolta R, Cosmacini P, Pignataro L, Castagnone D. Salivary gland stones: US evaluation in shock wave lithotripsy. *Radiology* 1997; 204:437–441.
 32. Gundlach P, Hopf J, Linnarz M. Introduction of a new diagnostic procedure: sialendoscopy (sialendoscopy)—clinical evaluation of sialendoscopy, sialography, and x-ray images. *Endosc Surg Allied Technol* 1994; 2:294–296.
 33. Marchal F, Dulgerov P, Lehmann W. Interventional sialendoscopy (letter). *N Engl J Med* 1999; 341:1242–1243.
 34. Marchal F, Becker M, Lehmann W, Dulgerov P. How I do it: interventional sialendoscopy. *Laryngoscope* 2000; 110:318–320.
 35. Dillon WP. MR sialography? *AJNR Am J Neuroradiol* 1998; 19:1183.